KinPhy: A Kinetic In-Band Channel for Millimetre-Wave Networks

Mohammed Alloulah[†] Zoran Radivojevic[†] René Mayrhofer[‡] Howard Huang[†]

[†]Nokia Bell Labs [‡]Johannes Kepler University

ABSTRACT

We propose a system for enabling auxiliary communication channels in which a node transmits a millimeter (mm) wave signal which is reflected off a deliberately vibrating surface of a second node and then received by the first node. Data sequences can be encoded in the modulation of the surface, and radar sensing techniques can be used to demodulate the reflected signal. Hence our system enables not only conventional sensing in terms of range, velocity, and orientation estimation but also allows for information to be conveyed by the sensed device. We introduce the design of a metasurface driven by an energy-efficient programmable piezo-electric actuator, detail suitable radar processing, and characterize the link performance of the kinetically induced channel at distances up to five meters. As this metasurface could be used for both mobile devices and infrastructure devices, we describe opportunities for enabling novel capabilities including secure device authentication and extended-range wireless sensing across multiple devices.

CCS CONCEPTS

• **Networks** → **Cognitive radios**; **Wireless access networks**; *Wireless access points, base stations and infrastructure*; *Mobile networks.*

KEYWORDS

Millimetre-Wave, 5G

ACM Reference Format:

Mohammed Alloulah, Zoran Radivojevic, René Mayrhofer, and Howard Huang. 2019. KinPhy: A Kinetic In-Band Channel for Millimetre-Wave Networks. In *The 17th ACM Conference on Embedded Networked Sensor Systems (SenSys '19), November 10–13, 2019, New York, NY, USA.* ACM, New York, NY, USA, 11 pages. https://doi.org/10.1145/3356250.3360039

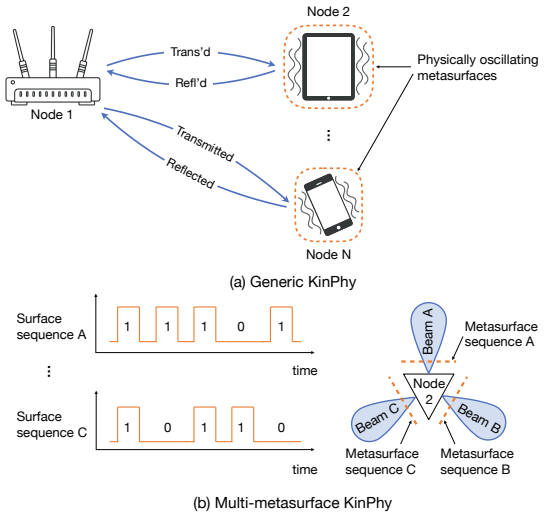

Figure 1: The combination of in-band mm-wave radar and physical vibrations forms a new kinetic channel for next generation WLANs whereby sensed objects can encode information back to a wireless device. (a) a generic illustration of KinPhy, (b) a generalized case in which different sides of a sensed object have individualized information-bearing vibrations corresponding to different mm-wave beam alignments.

1 INTRODUCTION

Growing demands for wireless communication capacity have catalyzed the adoption of millimeter-wave frequencies for both fifth generation (5G) cellular networks based on the 3GPP standard and future local area networks (LANs) based on the IEEE 802.11ad standard. The higher frequency range (30GHz to 300GHz), well above the single-digit GHz frequencies used for previous generations, presents opportunities for significantly higher data rates due to vast spectral resources. In 802.11ad networks, 2GHz bandwidth channels in the 60GHz frequency range will enable multi-gigabit per second data rates [33], and similar data rates and bandwidth allocations are expected in 5G systems [2].

In addition to communications, the radio spectrum can also be used for characterizing aspects of the physical environment via passive radar sensing. There have been works and commercial systems applying radar techniques indoors both in the sub-6GHz radio and mm-wave bands to demonstrate new capabilities such as sensing emotions [53] and vital signs [3, 26, 43]. In sensing applications, the vast mm-wave bandwidth resources enable finer spatial resolution so that even more subtle movements can be characterized. Indeed, mm-wave radar's advantage outdoors is such that level 5 autonomous driving may almost wholly be achieved by a dense 4D radar scanning in range, speed, azimuthal and elevation angles.

In this paper, we propose to extend the conventional concept of radar sensing by introducing a physically oscillating component. We describe a general scenario, shown in Figure 1(a) for two generic nodes and later provide details for a secure authentication application. In a conventional sensing system, node 1 would transmit

SenSys '19, November 10–13, 2019, New York, NY, USA

ACM ISBN 978-1-4503-6950-3/19/11…$15.00
https://doi.org/10.1145/3356250.3360039

a sensing signal (e.g., a chirp signal), and the reflection off node 2 would be received by node 1. By correlating the received signal with the transmitted chirp and performing additional baseband processing, the receiver can simultaneously estimate the distance, velocity and angle of node 2 with respect to node 1 [6]. Our proposal introduces a physically oscillating metasurface for node 2 that can be programmed to oscillate with encoded data sequences, for example using phase-shift or on-off keying.

This proposal is very general in that the sequences could be known at node 1 or they could be chosen from a codebook, as they might be in a conventional communication scenario. In addition, each node could be either a mobile or an infrastructure device. We call such system *KinPhy*: a *kinetic physical layer*. We now briefly describe three use cases enabled by KinPhy.

(i) Device authentication through haptic vibration sensing. Suppose in Figure 1 that node 1 is an access point and node 2 is a device that is requesting a connection with it. Following an initial access for beam alignment (e.g., (iii) below), a dedicated spatial channel can be set up between the nodes, and bi-directional information could be communicated using metasurface modulation for the purpose of device authentication. Compared to conventional authentication over an attack-prone wireless communication channel [**?**], authentication using the physically-actuated directional auxiliary channel could enable a significantly more secure authentication procedure, suitable for, e.g., connecting to devices that the network has no prior knowledge of [24], or to guard against beam stealing attacks [**?**]. We elaborate further on this important use case in §8.1 and provide a sketch of a KinPhy-enabled authentication protocol.

(ii) Sensing with extended range. In Figure 1, suppose that node 2 is to be sensed and its metasurface is modulated using a single sequence known at node 1. The total received energy and hence the sensing range can be increased by demodulating sequences of longer duration. In particular, pseudonoise spreading code sequences could be assigned to different sensed devices to enable unique identification and code multiplexing among the devices. Hence multiple devices could be sensed simultaneously using this technique. In §7.3, we demonstrate such extended range sensing in non-line-of-sight (NLOS) scenarios.

(iii) Rapid mm-wave beam alignment. As shown in Figure 1(b), different metasurfaces of node 2, each corresponding to a different beam direction, could oscillate with different sequences. If these sequences are known at node 1, then it could perform a correlation with each of the sequences to reveal the strongest reflected signal, indicating the most favorable beam generated by node 2. This procedure could work reciprocally so that node 2 could determine the best beam generated by node 1. Overall, this procedure would eliminate the need for the conventional beam alignment protocol that measures the SNR of each beam combination.

Generally, other applications can also benefit from KinPhy channels especially in areas such as Internet of Things (IoT), wearable security, mobile payments, and spontaneous secure interaction [22**?**].

While the performance of any such capability could be individually analyzed, this paper focuses on first steps towards a characterization of the received SNR as a function of the metasurface encoding sequence, distance between nodes, orientation of nodes, and utilized sensing bandwidth. The performance of all capabilities depend on this fundamental SNR metric, and we show how a sufficiently high SNR can be achieved in practical indoor environments.

Contributions. This paper describes the following contributions.

- To the best of our knowledge, this is the first paper to propose a system for in-band communication and sensing of radio signals that measure reflections off objects whose surfaces are physically modulated to encode information.
- We develop a class of novel, programmable vibrating metasurfaces using a piezo electric stack actuator.
- We pair our metasurface design with a custom radar signal processing pipeline. We show that the sensing of reflected mm-wave signals can be achieved reliably up to a distance of several meters.
- We also demonstrate that mm-wave sensing can be used to detect haptic vibration patterns from conventional smartphone devices, thereby lowering the adoption barriers of KinPhy significantly given the widespread of such built-in capability across modern personal devices.

2 RELATED WORK

KinPhy is inspired by past works belonging to two main bodies of literature: communications and sensing. However, KinPhy is the first system to recognize and demonstrate that mm-wave communication networks can benefit from a kinetic aiding channel that is in-band yet orthogonal to the standard operation of electromagnetic communication signals.

Communications. There is a variety of existing research that has utilized sensing modalities to enhance or augment mm-wave communication systems. Such sensing modalities have been used to help with the network's (i) setup and maintenance, (ii) security, and (iii) perception of the surrounding environment. One strand of research focuses on assisting mm-wave WLANs such as 802.11ad using orthogonal modalities. For instance, LiSteer performs beam setup and maintenance for access points using LEDs as an optical aiding modality [12]. Additionally, work by Ravindranath et al. presents a wireless protocol that integrates sensor hints from orthogonal modalities for the network's adaptation [30]. A similar idea is specialized further for managing the mobility of 60GHz WLANs and their beam tracking using accelerometer and magnetometer sensors [51]. Another strand of research aims to achieve dynamic sensing capabilities, similar to those using orthogonal modalities, while relying on in-band measurements from within the network link only. For mm-wave, examples of such in-band sensing capabilities include [20, 27, 50]. KinPhy bridges the gap between orthogonal modalities and in-band sensing in order to improve the latter while affording the advantages of the former. For example, orthogonal modalities are specifically beneficial to authentication but usually require hardware resources beyond the built-in capabilities of wireless networks e.g. ultrasound [24]. KinPhy has an in-band, yet orthogonal kinetic channel that leverages mm-wave radar and the ubiquitous haptics of modern devices.

Vibrational communications have also been reported, however as enabled by a contact accelerometer-based channel in [**?**] or contactless through the use of microphone-based sensing in [**?**]. In contrast, KinPhy is wireless radio-based which would allow for truly contactless and untethered vibrational communications.

Backscatter devices passively modulate incoming radio energy, commonly through changing their (scattering) antennae impedance, in order to signal information back to the originator of radio energy [**? ? ?**]. KinPhy follows similar system topology, albeit using a mechanical backscatter "twist." Firstly, such mechanical backscatter maps directly onto the haptic capabilities of modern personal devices. Secondly, a future tri-band router with a 60GHz sensing mode could play the role of a KinPhy reader [**?**].[1] As such, no additional mm-wave provisions—e.g. PIN diodes and MEMS [**? ? ?**], liquid crystals or ferro-electric films [**? ? ?**], or even graphene-based [**?**]—would be necessary for a covert backscatter channel to work. Our reported results herein could inform how vendors may choose to evolve mobile haptic core capabilities in the future to support KinPhy channels. That is, we believe KinPhy provides a simple and cost-effective pathway of convergence between mm-wave backscatter and haptics for applications where low bitrate and enhanced security are primary design goals.

Sensing. The research theme of wireless sensing has intensified over the past few years. Particularly, radar sensing is one subtheme that has seen research and indeed commercial activity on new compelling capabilities such as measuring human vital signs indoors over Wi-Fi and adjacent frequencies [1, 26, 53], and mm-wave frequencies [3, 43]. Radar-based gesture recognition and material sensing have also been reported [19, 49, 52]. Wireless vibrometry over sub-6 GHz frequencies has also been demonstrated as an acoustic attack vector [**?**]. Parallel developments outdoors, in the context of the autonomous vehicle initiative, have been fuelling radar-related research across analog and mixed-signal integrated circuit (IC) design [10], sophisticated target tracking schemes [11], to machine learning (ML) aided inference and decision-making [21]. KinPhy also uses radar, albeit for different sensing objectives, accompanying design techniques, and performance. KinPhy treats vibrational encoding and decoding at realistic indoor distances. Specifically, unlike material texture or hand gesture classification using ML [19, 49, 52], KinPhy relies on active haptics and man-made modulating signals that can withstand harsh indoor propagation. Indoor human vital sign sensing (e.g. [1, 3, 26, 43, 53]) shares the use of radar techniques generally but is tailored for larger human targets, larger-scale human breathing effects, and has no kinetic design component. KinPhy is inspired by high-end automotive radar; however, KinPhy also departs in its processing pipeline and general system architecture to cater for physical network sensing using minute haptics at micrometers scale.

Straddling both the communication and the sensing worlds, TARF is a recent close system that applies similar mm-wave sensing of vibrations to the problem of water-to-air communications [44], paying particular attention to underwater propagation nuances. In contrast, KinPhy deals mainly with the problem of over-the-air mm-wave vibration sensing and is designed to propagate over several meters as opposed to tens of centimeters in TARF [44].

3 KINPHY OVERVIEW

KinPhy recognizes the opportunity of transitioning WLANs into mm-wave frequencies. Given the much enhanced bandwidth and spatial resolution compared to previous generations, a sensing function can be built into the network using radar techniques at the physical layer. Such a sensing network function, when paired with the physical coding of objects using ubiquitous haptics, would allow native physical sensing of networked devices. Fundamentally, as shown in Figure 2, this new system is comprised of:

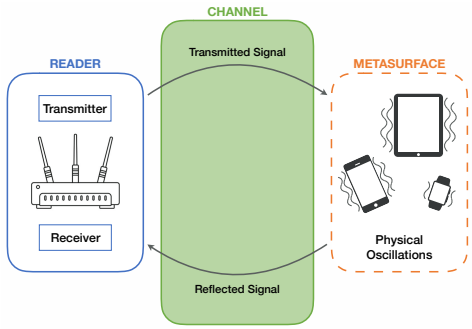

Figure 2: A kinetically-actuated physical layer sensing system consisting of a 60GHz reader transceiver device whose signals propagate through a wireless channel to impinge on a metasurface with encoded vibrations. Echoes reflected back enable the the decoding of vibrational information, bringing about possibilities for many network discovery, configuration, and management applications.

- Reader: A network node equipped with a 60GHz transceiver sends signals including but not limited to linear frequency modulation (LFM) [6] that reflect off surrounding objects in the environment to detect micro-Doppler effects arising from surface vibrations [7]. These micro effects enable the demodulation of vibrational information.
- Metasurface: A network node has a physical surface, such as a smartphone screen, that can actuate vibrational information. Current haptics support low frequencies in 100's of Hertz designed to interact with human tactile senses. In material science circles, such a physical surface is labelled a metasurface [8, 17, 35].
- Channel: An indoor space of several meters through which mm-wave signals propagate a round-trip distance.

In what follows, we describe our KinPhy system. We begin by reviewing the channel model, followed by a detailed discussion of the metasurface and reader principles.

4 THEORETICAL UNDERPINNINGS OF KINPHY CHANNELS

KinPhy is a new in-band channel that has potential to aid and complement the operation of a standard 802.11ad network. However, a number of theoretical underpinnings govern the effective harnessing of KinPhy in a future incarnation of 802.11ad. In what follows, we discuss these underpinnings.

4.1 Range

The Friis transmission equation $P_{\text{rx}} = P_{\text{tx}}\left(\frac{\lambda}{4\pi D}\right)^2 G_{\text{tx}} G_{\text{rx}}$ for a radio system relates the received power P_{rx} to the transmitted power P_{tx} at a pair of transmit-receive antennae operating at a given frequency wavelength λ [4].[2] Specifically, the received power depends on the

[1] 1st generation tri-band routers are already commodity devices.

[2] Similar principle applies to multi-antenna systems.

distance D between the antenna pair as well their respective radio chain gains G_{tx} and G_{rx}. For a radar system that listens to reflected echoes travelling a round-trip distance, we can specialise the Friis equation as [**?**]

$$P_{\text{rx}} = P_{\text{tx}}\left(\frac{\lambda_c^2}{(4\pi)^3 R^4}\right) G_{\text{tx}} A_{\text{tg}} G_{\text{rx}} \tag{1}$$

where R is the range to a target, and A_{tg} is a target coefficient that determines how much power is reflected back to the radar as per the target's radar cross section (RCS) and geometrical factors e.g. angles of incidence and reflectance. RCS is a measure of how much a target illuminated by radio energy reflects some of this energy back to the radar. For a radar system operating in the 60GHz band, typical small indoor objects have improved abilities to reflect electromagnetic energy compared to the Wi-Fi sub-6GHz band. This is because small objects are better reflectors of the fine 60GHz wavelength. For instance, a plate has an RCS given by [36]

$$\sigma = 4\pi A^2/\lambda_c^2 \tag{2}$$

For a 10cm-side square, the RCS expressed in decibels square metre is around 16dBsm for a 60GHz carrier compared to −4dBsm for a Wi-Fi carrier. Such new-found capabilities present opportunities to conduct space auditing for indoor environments at unprecedented scales.

Thus from equation (1), for a finite transmit power, fixed antenna gains, and a certain target electromagnetic reflectivity characteristics, the amount of received power is inversely proportional in $4th$ power to how far the target is relative to the radar system. Indeed, the Cramér-Rao bound (CRB) for estimating the range r of a target using an LFM radar can be shown to be [6, p. 299]

$$\text{CRB}(r) = \frac{3}{2(2\pi)^2 \text{SNR}}(\Delta r)^2 \tag{3}$$

and a similar expression appear for velocity i.e. range rate.

The lower bound of equation (3) shows inverse proportionality to the target SNR, and proportionality to the radar system range resolution $\Delta r = c/2B$ which is in turn determined by the utilised bandwidth. Again, operating under fixed transmit power, radio chain gains, and target reflectivity behaviour, the inverse proportionality on SNR appearing in CRB(r) becomes attributed mainly to the range-dependent attenuation term λ_c^2/R^4. That is, the farther the target is, the worse is our ability to estimate its distance.

Given mm-wave's limited ability to diffract around objects and a quasi-optical propagation, opportunities to extract diversity gain from multipath arrivals are reduced compared to sub-6GHz frequencies. As such, paying attention to the distance-dependent attenuation depicted becomes especially important. In fact, for indoor applications, state-of-the-art commercial radar vendors such as Vayyar [46] supply per voxel "soft information" to accompany and qualify output radar 3D images. We will comment later on how SNR can be estimated in practice from within radar processing pipelines.

4.2 Range Phase

We refer to the phase of a stationary target which may or may not change in time as range phase. When a target minute displacement is insufficient to change the discrete radar range estimate—i.e. a DFT bin location—the received radar LFM signal is modulated with a phase term proportional to the minute displacement. Concretely, the LFM waveform is defined as $s(t) := \exp(j\pi \frac{B}{T} t^2)$, where B and T are respectively the chirp bandwidth and duration.[3] It can be shown that the received beat is [6]

$$b(t) = a \exp\left\{j2\pi\left(2\frac{f_c}{c}\dot{r} + 2\frac{B}{Tc}r\right)t\right\} \tag{4}$$

where c is the propagation speed of light, again B and T are respectively the chirp bandwidth and duration, a is a scaling constant, f_c is the carrier frequency, r is the target's range, and $\dot{r}$ is the target's range rate i.e. velocity or vibration. The chirp duration T can be made substantially faster than the rate at which $\dot{r}$ changes. This allows for *decoupling* the contributions of r and $\dot{r}$ to the beat phase. As such, detection becomes two-dimensional: (i) in *fast-time* to estimate the range r, and (ii) in *slow-time* at range peaks to estimate the range rate $\dot{r}$. In a KinPhy channel where the target is stationary i.e. has constant r, the phase modulation term reduces to

$$\phi_r(t) = 4\pi\frac{\delta r(t)}{\lambda_c} + \phi_{r_0} \tag{5}$$

That is, sub-wavelength displacements translate into phase modulations at a given range peak r. Dubbed the Micro-Doppler effect, such phenomenon has been formally introduced and studied in prior art [7].

The phase modulation of equation (5) allows us to *code* the otherwise stationary physical objects with unique vibration patterns. However, our ability to *decode* $\phi_r(t)$ is clearly contingent on detecting r first. Note that the requirements of conventional radar sensing mostly concern estimating r and *multi-wavelength* $\dot{r}$. KinPhy departs from conventional radar sensing by requiring high-fidelity $\phi_r(t)$ estimation. Moreover, such range phase estimation has been shown to be governed by a CRB of its own, which unsurprisingly is also inversely proportional to SNR [34]

$$\text{CRB}(\phi_r) \propto \frac{1}{\text{SNR}} \tag{6}$$

A KinPhy channel is therefore doubly nuanced in that SNR variabilities affect both range and range phase estimates. In relation to the latter, KinPhy is characterised by increased phase instabilities the farther the coded surface is. In the following sections, we incorporate the characteristics we exposed above into the design and implementation of signalling strategies that are able to compensate for real-world, distance-dependent SNR losses.

5 KINPHY OSCILLATING SURFACE

The objective of KinPhy's physical modulation component is to induce a phase modulation pattern as per Equation (5), while maximising the wireless link budget cf. Equation (1). In order to achieve such design objective, we turn to the field of material science.

Typical metasurfaces are reflective surfaces realised by conductive periodic structures of subwavelength features in dimension, deposited on dielectric substrates or apertures engraved into metallic sheets [8]. Metasurfaces raised significant scientific attention due to their properties such as negative or near-zero refractive index [35], anomalous reflection, focusing and cloaking phenomena [17]. A

[3] Note instantaneous frequency $f_{\text{inst}} = \frac{1}{2\pi}\frac{d}{dt}\phi(t) = \frac{B}{T}t$, and hence the term linear.

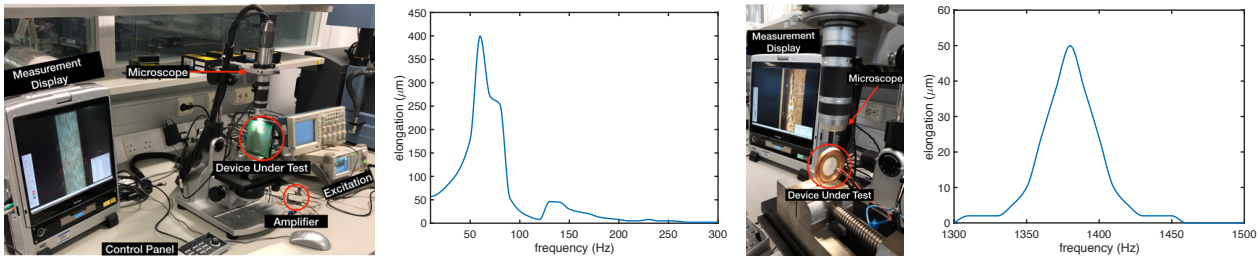

(a) Bi-morph (b) Bi-morph frequency response (c) Brass disc (d) Brass disc frequency response

Figure 3: Characterising elongation amplitudes of the vibrating surfaces at different frequencies by focusing an optical microscope on the side of the vibrating surface. (a) Metasurface suspended on four bending piezo actuators. (c) A single piezo actuator module hard glued to metallic brass disc.

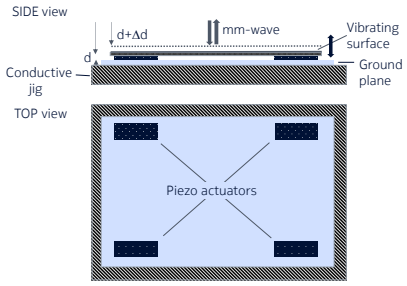

Figure 4: Schematic of programmable vibrating metasurface prototype.

metasurface can be designed and engineered to effect a reflection phase for impinging electromagnetic waves. This makes them attractive for advanced applications such as adjustable resonant antennas, polarization converters, holographic surfaces, etc. [47]. Some of these tuneable surfaces utilise micro-electromechanical systems [5], liquid crystals, or linear piezoelectric actuators for the dynamic control of the surface properties for, say, phase shifting at high frequencies. However, ordinary linear piezo actuators have relatively limited displacements, typically in the range of few micrometres.

In this work, we have used an array of novel programmable multi-layered piezo electric stacks capable of delivering significant displacement—i.e. a few hundred micrometres—at relatively low supply voltage (tenths of volts). The piezo electric stack actuator is made in a form of a bi-morph mechanical structure which significantly amplifies the elongation amplitude. As shown in Figure 4, we used four such piezo actuators to program dynamically the electromagnetic features of our adjustable metasurface antenna (AMS) prototype. Specifically, dynamic modulation is achieved by employing four piezo bi-morph actuators capable of delivering hundreds of micrometre displacement under programmed AC or DC biasing. Such displacement is significantly higher when compared to previously reported linear piezo actuators [39].

Surface design & prototyping. We have experimented with several types of programmable metasurfaces. Different metasurfaces were realised by depositing conductive layers on dielectric substrate (1.5mm thick epoxy fibre-glass FR4) with $\epsilon_r = 4.7$ and $\tan\delta = 0.017$ placed at distance $d = 0.5$mm from a ground plane. The first version of the metasurface included 25 micrometres thick homogeneous aluminium layer. The second version metasurface was realised in a matrix form made of basic copper elements 35 micrometre thick metallic square loop elements. Periodicity of the matrix structure is $p = 2$mm, the outer dimension of the square loop is $q = 1.8$mm, the inner circle gap dimension is $s = 1$mm.

Initial cavity thickness between the substrate and the ground plane was set to $d = 0.5$mm. The third type of the metasurface was realised by using a piezo-ceramic disk (30×0.2mm) hard-glued to brass metallic disc (dimensions of 50×0.1mm) which is rim-framed in a copper ring to enable more intensive confocal flexing of the brass disc surface. The entire assembly was then hard glued with an insulating ring to backing ground plate made of 20 microns thick aluminium layer on the epoxy fibre-glass. We should point out that the performance of the metasurface is related to the resonance of the open cavity formed between the conductive structures and the ground resulting in a strong dependence of the reflection phase on the cavity distance d.

The final design iteration features a 90×95mm metasurface that is suspended by four bi-morph piezoelectric actuators located at the assembly corners as shown in Figure 4. By varying the excitation signal of the actuators, the movement is translated to a vertical displacement of the metasurface w.r.t. the ground plane. At bottom of the substrate and in a proximity to the conductive elements there is a ground plane. As it can be seen in Figure 4, the actuators are located around the metasurface corners, which does not interfere with the radiation performance and thus results in a very low loss structure. When four of the actuators are simultaneously excited, a displacement of the metasurface is produced thereby changing the distance between the conductive layers and the ground. Such displacement results in a change of the reflection phase response of the metasurface structure. The actuators were driven by piezo amplifier (E-835 PI) fed by analogue signals from a PC. The driving signals on the PC were generated by using AVS4 and LabView source codes. The amplification factor of the PI was 25× leading to 25V peak-to-peak (Vpp) excitation signal for the piezo actuators.

By adjusting the excitation signals of the piezo bi-morph actuators, we can tune the electromagnetic reflectivity of the metasurface dynamically. That is, modulating the actuators' excitation signal allows us to change the *phase* of the reflected electromagnetic wave programmatically.

The physical modulation of our adjustable vibrating metasurface is based on the use of four modules of bi-morph type of piezoelectric bender actuators which dynamically change the cavity thickness of the metasurface. Therefore, the maximum modulation range of the structure is determined by the maximum displacement produced

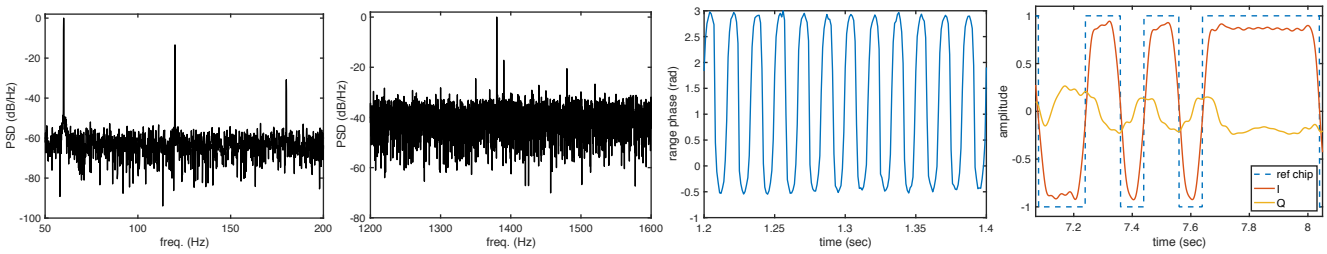

(a) Bi-morph (b) Brass disc (c) Bi-morph's range phase (d) Bi-morph's pseudonoise sequence

Figure 5: Power spectrum densities for the two metasurface variants: (a) Bi-morph, and (b) Brass disc, at their respective resonance frequencies. (c) depicts a snapshot of bi-morph's range phase under LOS conditions and at 5m distance. (d) depicts a snapshot of bi-morph's demodulated spread spectrum chips.

by the actuators. We used TDK PHUA3015-20A bi-morph actuators [40]. Such actuators are made of a piezo-ceramic block on a metallic plate (42Ni-Fe) with dimensions $30 \times 15 \times 0.1$mm, respectively. The actuators have very quick response and can achieve fast transients operating at ultrasonic frequencies (> 20kHz). Large elongations produce displacements of the metasurface up to 500 micrometres. The piezo-ceramic block is built from multiple layers of ceramic plates placed on top of each other forming a piezo stack. The piezo stack is then hard-soldered on a metallic plate whose mechanical resonance is tuned to empathize mechanical bending further. Each ceramic layer has the property of expanding when exposed to positive electrical potential, due to the piezoelectric phenomenon. Different voltages are applied to the upper and lower layers through two electrodes (+V, 0) provoking an expansion to the upper layer, which in turn causes extensive bending of the piezo bi-morph structure. Such operation creates a bending of the piezo actuator, similar to the principle of thermostatic bimetals that translate the small change in the length of the ceramic plates into a large vertical displacement. The total displacement of a piezoelectric actuator depends on its total length.

Surface characterisation. The vibrating metasurfaces were characterised by using optical microscope focused on the side of the metasurface plane as shown in Figures 3(a) & 3(c). In all tests, metasurfaces were fixed vertically giving good access and side-visibility to the vibrating plane. A sweep type sinusoidal stimulation function was generated to excite the metasurfaces and microscope videoclips were recorded with calibrated elongations of the microscope images. The vibrating amplitudes were analysed offline resulting in the frequency response of the metasurfaces as depicted in Figures 3(b) & 3(d). The metasurface with four piezo bi-morphs showed several resonating peaks at frequencies of 60, 75 and 140 Hz, as can be seen in Figure 3(b). The metasurface with framed brass disc was stimulated with 16Vpp sinusoidal signals producing intense displacements with maximal amplitude of 50 microns at a resonant frequency of 1380 Hz, but exhibited relatively narrowband behaviour as shown in Figure 3(d). Therefore, given the larger elongation and wider bandwidth of the bi-morph metasurface, we will mainly use this variant for the end-to-end evaluation of our KinPhy system reported in §6.

Surface modulation. Findings from §4 have exposed the distance-dependent SNR variabilities of KinPhy channels. Such SNR variabilities call for a robust modulation scheme that can trade off spectral efficiency with extended range of operation. In mapping KinPhy's characteristics onto modern modulation schemes, we thus choose spread spectrum. As such, by varying spreading code length (e.g. Gold code), we can arbitrarily enhance SNR in order to combat distance-dependent performance degradations. In terms of robustness to noise, KinPhy channels share similar design objectives to the global positioning system (GPS) [15], ultra low-power body area network (BAN) radio communications with stringent link budgets [14], and more generally civil or military applications for low probability of intercept (LPI) [38]. A commonality between such applications is a requirement for a guaranteed level of performance under challenging operational SNR conditions. In addition, spread spectrum signalling allows for a scalable sharing of the channel through code division multiplexing with decode algorithms ranging in complexity from nuisance multi-user interference tolerance to successive interference cancellation (SIC). Figure 5(d) depicts a snapshot of demodulated complex chips[4] that demonstrate good mechanical phase transients.

6 KINPHY WIRELESS READER

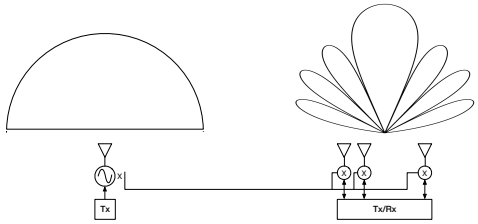

Figure 6: Architecture of a modified transceiver to support simultaneous communications & sensing.

We now turn to treat how a revamped future version of 802.11ad physical-layer can be made to perceive its environment natively, including but not limited to reading wirelessly coded KinPhy metasurface vibrations.

Architecture. A 60GHz mm-wave communication transceiver can be extended at marginal cost to mm-wave integrated circuit (MMIC) resources in order to support radar-type signalling. Specifically, Figure **??** depicts a modified MMIC architecture whereby provisions are made for a transmit antenna whose oscillator is coupled with that of the standard phased antenna array[5] used for 802.11ad. Typically,

[4]Demodulation details are treated in §**??**.
[5]and its analogue and mixed-signal circuitry

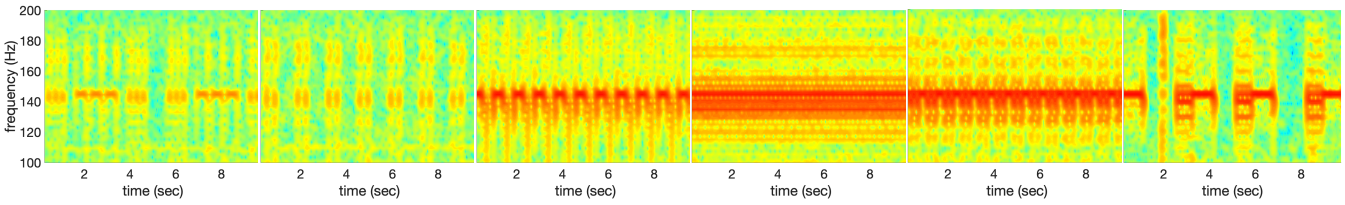

(a) SOS (b) Heartbeat (c) Accent (d) Rapid (e) Staccato (f) Symphony

Figure 7: Spectrograms for 6 iPhone X haptics.

for increased coverage, the additional transmit antenna is designed to have a wider beam lobe [25], or quasi-omnidirectionality altogether in the case of ubiquitous radar [37, 48]. Such marginal modifications to the MMIC architecture would make possible the reuse of the 802.11ad 60GHz band for sensing purposes. The Federal Communications Commission (FCC) has recently extended the 60GHz indoor band to a mighty 14GHz [9] and followed with relaxing some regulatory aspects around transmission power limits for sensing [31]. We recognise these recent trends and would argue that the time is opportune for a revisit of the 60GHz band's PHY capabilities in order to support new class of future radio devices capable of not only communications, but also high-fidelity sensing, simultaneously. Such radio architectural rethinking could open up the door for new possibilities such as the KinPhy channel we advocate for herein.

6.1 Illustrative experiments

We start our treatment of KinPhy reader by tying how it works intuitively and at a high-level to two concrete case studies: (i) a haptic use case using an off-the-shelf smart phone, and (ii) using the metasurface variants we designed in §5.

Haptic case study. In §4, we have treated the fundamental principles governing the KinPhy channel behaviour. Specifically, surface modulations imparted by physical vibrations of objects can be decoded by means of Equation (5). In order to provide intuitions for the notion of slow-time phase demodulation along with its CRB (cf. §4.2), we present next a case study of "reading" haptic vibrations of an iPhone X device over the KinPhy channel.

We conduct an experiment in which we mount an iPhone X on a tripod facing the boresight of a 60GHz radar.[6] Whilst on silent mode, the iPhone number is called triggering its vibrations, and simultaneously the radar mm-wave sensing commences for approx. 10 seconds. The experiment was repeated for six iPhone X haptic patterns: sos, heartbeat, accent, rapid, staccato, and symphony. For patterns sos and heartbeat, the distance between the iPhone and radar was approx. 1.5m. For the rest of the patterns, the distance was approx. 1m. We perform radar processing and extract the phase modulation corresponding to the vibrating iPhone target from one receive antenna only.[7] In the interest of visualisation, we obtain the spectrograms for the vibration phase modulation term cf. Equation (5). Results are shown in Figure **??**. It is evident that these various haptics illuminated by a 60GHz radar represent an off-the-shelf demonstration of KinPhy channels. Range phase demodulation as per Equation (5) is able to discern the subtle surface vibrations induced by various haptics; Together, the iPhone X glass and form factor act as a good mm-wave reflector. Specifically, with the dimensions of the iPhone in mind (143.6×70.9mm) and recalling Equation (2), its RCS is approx. 17dBsm. This case study provides early indications that phone form factors are ample targets for KinPhy channels. Note, however, how sos and heartbeat experiments judiciously placed 0.5m farther than the rest have somewhat *fainter* red colour intensity. This observation is in agreement with Equation (6); namely, that KinPhy's sensitivity to range phase drops in distance. We will corroborate this early result in §7 and demonstrate how such performance drop can be mitigated against using robust spread spectrum coding.

Metasurfaces case study. We now return to the two prototype metasurfaces we built and characterised in §5. The aim is to demonstrate that KinPhy is a viable in-band channel for future indoor mm-wave networks through a first end-to-end (metasurface + reader) KinPhy experiment.

To this end, we repeat the experimental setup of the previous haptic use case swapping the iPhone for our KinPhy prototype metasurfaces. The bi-morph and brass disc metasurface variants were respectively placed 5m and 1.5m away from the radar while facing its boresight. That is, the metasurfaces were perpendicular to the line-of-sight (LOS). Recall from §5 the geometries of the bi-morph and brass disc variants: a 90×95mm rectangle for the former and a 50mm-diameter circle for the latter. Plugging the areas into Equation (2), we obtain RCS's of approx. 15dBsm for the bi-morph and 3dBsm for the brass disc. Pure sinusoidal excitations where generated for both at the resonance frequencies of 60Hz and 1.38kHz as per Figure 3. A back-off of 5V from bi-morph's 25Vpp maximum excitation was used for thermal management of the driving amplifier, lowering the corresponding maximum elongation by 1/5th to around 300μm. Full 16Vpp dynamic range was left for the brass disc. Again, we perform radar processing and extract the phase modulation corresponding to the vibrating metasurfaces from one receive antenna only. The corresponding power spectral densities (PSDs) are shown in Figures 5(a) & 5(b) along with a snippet of the raw range phase of the bi-morph in Figure 5(c). In line with its frequency response of Figure 3(b), bi-morph's response comprised of a main harmonic at 60Hz followed with two attenuated images at 120 and 180Hz. Total harmonic distortion (THD) without filtering was better than −13dB, although around −60dB can be achieved. Comparatively, the brass disc's response to its 1.38kHz resonance pure sinusoidal excitation was cleaner with THD better than −17dB. However, owing to a much reduced RCS, the brass disc PSD noise floor was 20dB higher than

[6] Details of our experimental radar testbed will be given in §6.
[7] KinPhy's processing pipeline will be discussed thoroughly in §**??**.

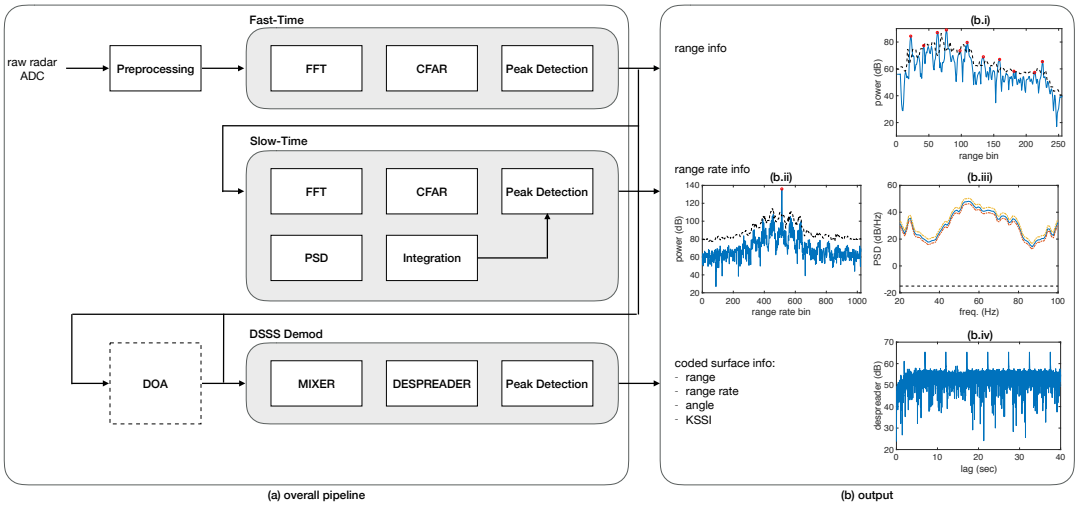

Figure 8: KinPhy sensing pipeline alongside snapshot examples of various detection stages.

that of bi-morph even when its distance from the radar was 3.3× closer compared to bi-morph. Nonetheless, we have demonstrated that a variety of metasurfaces—iPhone, bi-morph, and brass disc—of differing geometries and material properties can be made to support our proposed KinPhy channel. In the rest of the paper, we will mainly present evaluation benchmarks using the bi-morph metasurface.

6.2 KinPhy reader processing pipeline

We now delve into the details of KinPhy's reader processing pipeline which enables (i) the scanning of the environment in search of objects with coded metasurfaces, (ii) estimating their range, velocity, and relative orientation, and (iii) decoding their unique vibration sequences to ascertain various object ID's present nearby.

As depicted in Figure **??**(a), KinPhy has broadly three flows: fast-time radar processing, slow-time radar processing, and a direct-sequence spread spectrum demodulator.

Fast-time. The notion of fast-time processing in radar literature refers to performing initial target detection in the range dimension. Recalling Equation (4), the baseband representation of the received beat is converted into peaks corresponding to hypothesized targets through a series of transformations starting with windowing & DFT[8], constant false alarm (CFAR) detector, and peak finding. We use a specific flavour of CFAR based on order statistics (OS) owing to its superior performance under realistic complex clutter behaviour and a better ability to estimate the SNR of hypothesized targets [32], which is distance-dependent as per the treatment in §4. The output of this stage is a list of hypothesized targets marked in red in the example range spectrum of Figure **??**(b.i). As can be seen, reflective surfaces and objects in indoor environments give rise to many *resovled* mm-wave radar echoes of various strengths. The dotted line represents the detection threshold arrived at by OS-CFAR.

Slow-time. In classic radar techniques, slow-time processing analyses the spectral characteristics of range targets across time in order to determine their rate of change and consequently their Doppler content. Radar's ability to measure such temporal rate of change is attributed to the $\dot{r}$ term in Equation (4). For KinPhy, we are interested in detecting and decoding minute surface vibrations. In the current version of KinPhy, coded objects are stationary i.e. have no Doppler/velocity content in the *kinematic* sense. This can be seen by noting the detected red peak midway across range rate bins in Figure **??**(b.ii). However, note the "blips" around the zero Doppler peak which the dotted black threshold of OS-CFAR skirts and deems as no peaks. These "blips" are due to phase spreading corresponding to a KinPhy metasurface's coded vibrations and would require a secondary detection flow. Thus, as depicted in the slow-time flow of Figure **??**(a), a parallel branch performs PSD estimation also in the slow-time followed by integration over the spread spectrum frequencies of interest. As illustrated in Figure **??**(b.iii), such PSD has significant DSSS energy which the KinPhy reader searches for in slow-time and across the frequencies of interest. When the KinPhy reader finds such DSSS energy, it flags to its slow-time peak detector that the stationary target OS-CFAR has found is likely to encode surface vibrations. This information is then communicated out to the subsequent DSSS demodulation flow.

DSSS demod. Once the target corresponding to a KinPhy metasurface has been identified through a series of fast-time and slow-time processing, the target's range bin index is passed to a DSSS demodulation flow along with the radar data cube. The DSSS demodulator proceeds then as follows. First, it slices the FFT'ed I/Q (real & imaginary) data at the target's range bin index across slow-time. Second, the sliced data is band-pass filtered, mixed down with a complex carrier at the designated frequency (e.g. 60Hz for bi-morph), and then low-pass filtered as per the chip rate of the spreading code (e.g. 25Hz for bi-morph). Third, the resultant mixed down and filtered signal is despread using the template code used by the KinPhy metasurface to encode its vibrations. Fourth, the running despreader output is monitored using an appropriate threshold for detecting the presence of peaks, concluding the demod flow. Figure **??**(b.iv) shows an example running despreader snapshot when a KinPhy metasurface using a 127 Gold code and 25Hz chip rate are used. The periodicity of detection corresponds to the approx. 5-second Gold

[8] performed efficiently as FFT

code duration.[9] Note that in relation to the complex despreader, the KinPhy reader operates on the I/Q data directly with no explicit demapping to phase in order to avoid potential interaction between noise and the nonlinear behaviour of inverse trigonometric functions, especially in a low SNR regime. An example of such low SNR regime can be seen in Figure **??** where it is clear that complex despreading outperforms real despreading operating on phase.

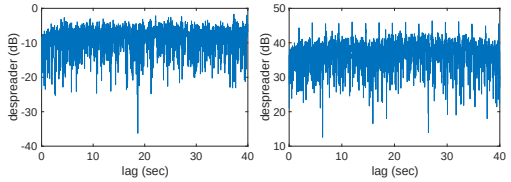

(a) `atan2` (b) I/Q

Figure 9: Low SNR regime comparison between **??** real despreader after `atan2` demapping, and **??** complex despreader operating on I/Q directly.

So far, we have treated the KinPhy processing pipeline without making reference to the multiple antennae of the mm-wave radar phased array. For reasons we will discuss in §8, we simply repeat the flow for each antenna element and aggregate detection results using a simple majority voting mechanism. At the end of KinPhy processing pipeline as highlighted in Figure **??**(b), information about nearby present modulated metasurfaces is complete in the form of estimates of: range, range rate, relative orientation, kinetic signal strength indicator (KSSI) obtained from despreader output, along with SNR from OS-CFAR.

We conclude this section by summarising the overall KinPhy sensing pipeline in Algorithm **??**.

Algorithm 1: KinPhy reader

```
input  : Radar cube of size N_rng × N_dop × N_ant, where the dimensions are
         # of bins in range, Doppler, and antennas, respectively.
output : Estimates of: range, range rate, DOA, KSSI, and SNR.
for receive antennas do
    look for targets in fast-time;
    for detected range targets do
        look for metasurfaces in slow-time;
    end
    for detected range-Doppler tuples do
        estimate direction of arrival;
    end
    for detected range-Doppler-angle tuples do
        demodulate slow-time I/Q at range bin;
    end
end
Aggregate results from all antennas.
```

7 EXPERIMENTAL EVALUATION

7.1 Testbed

KinPhy's experimental testbed consists of (i) a metasurface for actuating the coded vibrations, and (ii) a radar reader operating in the 60GHz band.

(i) Metasurface. The iterative design process for arriving at a suitable KinPhy metasurface was treated in §5. To recap, owing to its superior 15dBsm RCS, wider 50Hz bandwidth, and a higher

[9] We will discuss in §8.2 how spreading code latency can be lowered substantially in a future metasurface design iteration.

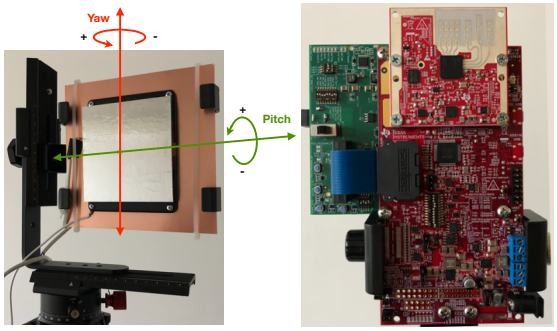

(a) Bi-morph metasurface (b) Radar

Figure 10: KinPhy's testbed: (a) Bi-morph metasurface, and (b) radar by Texas Instruments.

$\sim 300\mu$m elongation at 20Vpp excitation, the bi-morph variant was chosen for the empirical data collection campaign. The metasurface were driven by PI piezo amplifier E-835 [28] fed with a standard analogue audio output from a workstation running Windows. Excitation signals were generated as wav files and played on repeat for each test configuration. These configurations will be detailed in §6.2. In terms of DSSS signalling, a carrier at the 60Hz resonance frequency was used with a chip rate of 25Hz. We followed standard DSSS modulation and demodulation practices e.g. oversampling, pulse shape filtering, etc [15]. The 90×95mm bi-morph metasurface mounted on a panoramic camera tripod ball head with a 360° swivel indexed rotator and two-way rail slider is shown in Figure 6(a). As can be seen, the metasurface was covered with aluminium foil to enhance its reflectivity. The larger copper plate was used for electrical grounding purposes only.

(ii) Mm-wave Radar. We use an off-the-shelf FMCW 60GHz radar offering from Texas Instruments (TI). The offering is comprised of three subcomponents: (1) the IWR6843ISK mm-wave sensor featuring 3-transmit and 4-receive patch antennas along with integrated MMIC and baseband processing, (2) the MMWAVEICBOOST carrier interface card, and (3) the DCA1000 evaluation module for real-time Ethernet raw ADC acquisition and streaming [42]. This combined platform is shown in Figure 6(b). The IWR6843ISK sensor module is capable of supplying 10dBm transmit power. The radar has extensive signalling configurability which we exploit for our empirical evaluation. Specifically, we set the chirp pulse repetition interval to 80μs and use the two chirp slopes of 25MHz/μs and 50MHz/μs in order to configure the two bandwidth options of 1.75GHz and 3.5GHz. Note also that TI's radar supports a maximum of 255 back-to-back chirp transmissions due to a mandatory recalibration period, which would result in irregular sampling in slow-time. To work around this issue as well as fit real-time ADC streaming to available memory and Ethernet throughput, a single chirp frame was 8.7% duty-cycled to give an effective sampling frequency of 1kHz in slow-time. We use TI's mmWave Studio [41] which runs under Windows to configure and control the radar, as well as to acquire raw ADC data using the supplied Lua scripting [18] API.

Acquired raw ADC data is then imported into Matlab and passed to an implementation of the KinPhy reader treated in §**??** and whose pseudo code is summarised in Algorithm **??**.

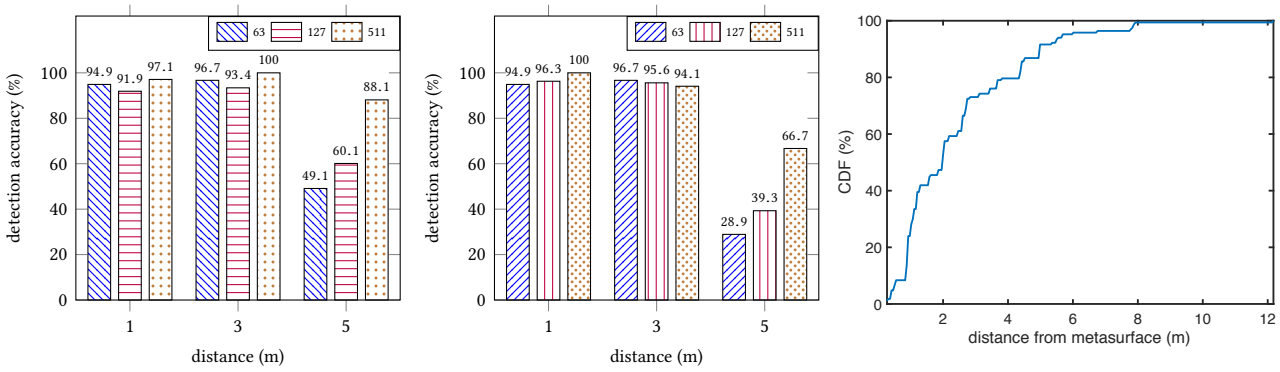

(a) (b) (c)

Figure 11: Aggregate detection accuracy as a function of distance, code, and bandwidth: (a) 1.75GHz and (b) 3.5GHz. (c) Demodulating from environmental NLOS echoes.

7.2 Evaluation

Setup. We evaluated KinPhy in an office environment whose floorplan is shown in Figure 8(b). The office has many other objects not shown in the floorplan such as computer monitors, plants, etc. In terms of wall material composition, the angled east wall is entirely made of glass, and so are the north internal partitionings and sliding doors.

Dataset. As depicted in Figure 8(b) and while always facing the boresight of the radar, the metasurface was placed along the dashed blue line at three distances: 1m, 3m, and 5m. Both radar and metasurface were mounted on tripods at a 2m height. The metasurface was wheeled on a mobile cart as depicted in Figure 8(a). In order to characterise angular effects on performance, the metasurface panoramic tripod mount shown in Figure 6(a) was rotated in yaw and pitch angles. Data acquisition scripts also varied a number of KinPhy performance critical parameters. Concretely, for each distance $d \in [1, 3, 5]m$, the following radar parameters and metasurface coding and angle combinations were tested:

- Bandwidth: [1.75, 3.5] GHz
- Gold code: [63, 127, 511] chips
- Yaw: [0, ±5, ±10, ±22.5, ±45, ±67.5, 90, 180]°
- Pitch: [0, ±22.5, ±45, ±67.5, 90]°

Consequently, experiment combinations totalled 378 tests. At each test configuration and depending on the length of the Gold code, 20, 40, and 80 seconds of raw radar data were recorded for code lengths of 63, 127, and 511, respectively. Thus the combined duration of the dataset was approx. 4.9 hours.

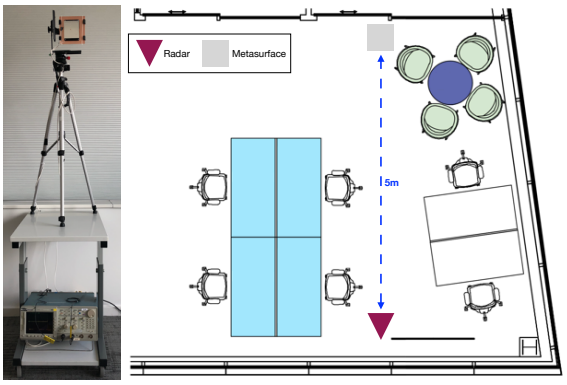

(a) Mobile cart (b) Office floorplan

Figure 12: Data collection in office: (a) metasurface on mobile cart, and (b) environment floorplan.

8 RESULTS

8.1 Microbenchmarks

We begin by providing an overall summary of how KinPhy's performance is impacted as a function of two key system configurations: spreading gain and utilised bandwidth. We conducted 378 tests as detailed in §6.2 in order to expose such performance dependencies.

(1) Distance. Distance is the main performance stressor of the ability to demodulate minute coded vibrations in realistic environments. In order to assess the influence of distance on the KinPhy reader, we compute a detection accuracy metric at each test distance aggregated for all yaw and pitch combination. This emulates an uncontrolled KinPhy operation in a given indoor environment whereby no optimal orientation can be assumed on the part of the metasurface—w.r.t. the KinPhy reader. Further, let us first examine such detection accuracy metric evaluated for Gold code length 63 and across distances 1, 2, and 5 metres as depicted in Figure 7(a). We note the following:

- Detection accuracy is in excess of 90% for distances 1 and 3m across all aggregated orientations, including very challenging cases such as Yaw 90°, 180° and Pitch 90°. E.g. Yaw 90° corresponds to the case when the metasurface is *facing away* from the KinPhy reader, and Pitch 90° corresponds to being parallel to the boresight of the radar. Successful detection under such harsh orientations, however, can be explained by nothing that coded vibrations are still being coupled e.g. to the metasurface copper plate for Yaw 180° and through the camera tripod mount for Pitch 90°.
- Detection accuracy drops to about 50% at 5m distance across all aggregated orientations. This is to be expected owing to decreased SNR at such long distance.

(2) Code. Spreading gain is one degree of freedom through which we can trade off spectral efficiency (or rate) for increased detection range. To further shed light on coding gain, we return to Figure 7(a) to examine detection accuracy across distance for three code options: 63, 127, and 511 chips. We note the following:

- In a *high SNR regime* corresponding to distances 1 and 3m, increased spreading gain has minimal effect on enhancing performance across aggregated orientations. Specifically, barring small statistical fluctuations, detection accuracy remains uniformly above 90% for the three code options.
- The benefit of increased spreading gain reveals itself at 5m distance under a *low SNR regime*. At 5m, enhancements to detection accuracy are brought about with added coding gain.

(3) Bandwidth. The amount of bandwidth utilised by KinPhy is important to consider. On the one hand, the current 802.11ad standard specifies 2GHz communication channels. On the other hand, short-range indoor radars for gesture interactions use up to 7GHz bandwidth for enhanced sensing. We want to understand the effect of bandwidth on our proposed KinPhy system. To this end, we now consider the aggregate detection accuracy metric while utilising two bandwidth options: 1.75GHz and 3.5GHz as shown in Figures 7(a) & 7(b), respectively. We note the following:

- In a *high SNR regime* corresponding to distances 1 and 3m—again barring statistical fluctuations, the two bandwidth options perform identically irrespective of doubling the bandwidth.
- In a *low SNR regime* corresponding to 5m, bandwidth 1.75GHz substantially outperforms 3.5GHz consistently across spreading codes. This empirical evidence suggests that confining sensing to within the already allocated bandwidth of the 802.11ad communication protocol is advantageous. KinPhy does not require finer distance resolution as afforded by increased bandwidth. At a deeper technical level, this can be understood noting that: (i) the phase spectrum of a range bin is flat around the true frequency bin, hence insensitive to estimation errors [34], and (ii) using less bandwidth improves the link budget over extended distances [45].

8.2 Angular KSSI

Next we study the kinetic signal strength indicator[10] (KSSI) as a function of yaw and pitch orientations and as measured at the despreader output. We want to understand how axial rotations in the metasurface affect the KinPhy reader's ability to decode vibrational information in a normal office environment.

(1) Yaw. Starting with Yaw, the upper row of Figure 9 shows the measured KSSI in polar coordinates for the three spreading code options of 63, 127, and 511, from left to right respectively. The standard deviation is indicated by lines at various orientations and distances. Note that for all angles, KSSI is steadily enhanced with spreading gain and also steadily decreases in distance. Therefore, spread spectrum is effective at combating SNR degradations not only in distance, but also in orientation, which is key for realising uncontrolled KinPhy operation indoors.

(2) Pitch. KSSI in pitch broadly follows the trends outlined for yaw. That said, inspecting the lower row of Figure 9 reveals an angular "blip" in KSSI around 45°. This might be due to interaction between complex indoor propagation and asymmetries in the beam profile. However, we plan to investigate this observation further in an anechoic chamber.

[10] as defined in §??

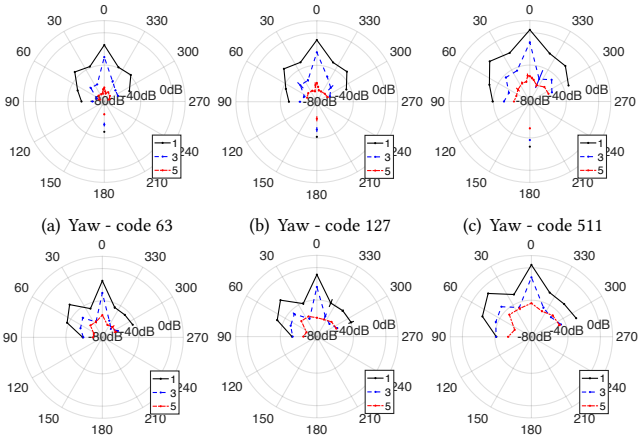

(a) Yaw - code 63 (b) Yaw - code 127 (c) Yaw - code 511

(d) Pitch - code 63 (e) Pitch - code 127 (f) Pitch - code 511

Figure 13: KSSI in yaw and pitch as a function of distance and across spreading code lengths.

8.3 NLOS Demod

So far we have detailed and characterised how KinPhy can demodulate the kinetic information from a target in sight of its radar reader. We now investigate if we can perform the demodulation flow on secondary reflections arising from complex and cluttered indoor environments. To this end, we define a mask around the range bins corresponding to the known metasurface distance. We then proceed to exhaustively search all remaining range bins having excluded the metasurface distance. The NLOS distances at which we successfully detect KinPhy-coded echoes are analysed in Figure 7(c), relative to the metasurface range.

Figure 7(c) shows that many successful *secondary* i.e. NLOS demodulations were possible across our dataset. Specifically, inspecting the cumulative distribution function (CDF) shows that 50 percent of these successful demodulations had originated from distances of 2m or less away from the metasurface. The 95th percentile of these NLOS echoes was under 6m in proximity to the metasurface, although echoes originating from distances as far as 12m away were detectable. This NLOS statistical analysis serves to demonstrate that significant range extension of traditional sensing can be obtained using KinPhy; KinPhy can literally bypass traditional CFAR radar detection to conduct brute-force search of coded surfaces present in complex cluttered environments.

9 DISCUSSION & LIMITATIONS

We discuss and remark on few relevant points to KinPhy.

9.1 Authentication - A Protocol Sketch

As mentioned in the introduction, such sensing capabilities on a tight-beam communication channel can potentially be utilized for authentication between involved devices. Similar to previous work on ultrasonic sensing [23], physical channel properties can

constrain adversaries to corresponding physical positions (i.e. range & orientation). Within the scope of this section, we therefore assume signal cancellation – or more generally, targeted manipulation of the reflected signal towards the original transceiver – is only possible within a sufficiently tight spatial sector. This implies an adversary model based on usual in-band and auxiliary channel characteristics (cf. [22]):

- Passive eavesdropping is assumed to be possible from arbitrary locations within the channel (i.e. typically room level as for ultrasound [23]). For KinPhy, this includes both in-band (data) communication during initialization/setup and auxiliary (kinetic) sensing, e.g. from multi-path effects of both the original and the reflected signals.
- Complete (active) denial-of-service is also assumed to be possible from arbitrary locations in range, but is detectable in the sense that communication is rendered impossible on the application level.
- Selective cancellation, manipulation, or injection of single packets or for single devices within the area is assumed to be prohibitively difficult unless the adversary is physically in direct line-of-sight between the two communicating devices (i.e. a physical man-in-the-middle).

Given these assumed adversarial settings, it seems fairly straightforward to construct an authentication protocol based on well-known primitives studied extensively for comparable threat models, even for the challenging combination of a modality that cannot be sensed by human users and without directly receiving user-controlled input [22]. While a complete authentication protocol design and analysis is out of scope of this paper, we suggest a protocol sketch for the sake of discussion:

a) Through pre-committed, ephemeral key agreement on the in-band communication channel, both devices create a shared session key that is confidential against passive eavesdroppers, but could be subject to an active man-in-the-middle attack on the in-band communication channel. Such key agreement is already supported in current 802.11 standards, particularly WPA3, which makes it likely that existing implementations in chipset firmware could be readily re-used.
b) In a secondary verification phase, a one-time secret deterministically derived from this shared session key is modulated on the KinPhy channel i.e. on node 2 metasurface and therefore transmitted to node 1 over kinetic mm-wave sensing. Based on the above adversarial model, this transmission may potentially be overheard from arbitrary positions, but cannot be manipulated by any adversary not physically in line-of-sight between the devices. Compared to previous work on ultrasonic positioning [24], modulation in KinPhy can be physically constrained with direction-of-arrival, and therefore be made even more resilient to various attacker locations.

This leaves an attacker a single chance to guess the one-time secret to remain undetected in a man-in-the-middle attack on the first phase. The probability for such an attack can be directly controlled through the length of the transmission in phase 2, resulting in a $1/2^n$ attack success rate for n bits modulated on the auxiliary sensing channel.

Finally, it is worth noting that compared to a symmetric cryptographic topology based on IEEE 802.11ad, modulation in KinPhy requires auxiliary (kinetic) mm-wave sensing for node 1 only along with auxiliary kinetic actuation (haptics) for node 2. As such, phase a) of the authentication protocol could even be implemented over a traditional sub-6GHz band, thereby further reducing the RF requirements of node 2. A full design and security analysis are subject to future work.

9.2 Limitations & Research Directions

Our first KinPhy prototype can be invariably improved upon both in relation to the metasurface and the radar reader. The former would allow much increased data rate while the latter would enable the evaluation of uncontrolled applications built on top of KinPhy. Therefore, both items warrant significant further research.

(a) Metasurface 2.0. Our Bi-morph metasurface prototype is based on off-the-shelf haptic actuators. As such, resultant kinetic modulation rate is relatively slow i.e. 60Hz carrier and 25Hz chip rate. However, kinetic modulation can be made orders of magnitude faster using other materials such as Polyvinylidene Fluoride (PVDF) [16] since KinPhy need not interact with human tactile senses, but only reflect massless mm-wave energy. Indeed, similar wideband transducers for ultrasonic localisation have been demonstrated with long spread spectrum signalling lasting 25ms only [13] and compactly integrated in a stylus product [29].

(b) Dense radar scanning. Our current evaluation of KinPhy is gated by the advent of dense 60GHz antenna arrays capable of sophisticated receive and/or transmit beamforming in order to conduct wide-coverage space auditing of metasurfaces. Early findings indicate commendable resilience to axial (i.e. yaw and/or pitch) misalignment through SNR-boosting spread spectrum coding. A future research direction would refine coarse detection under misalignment through beamforming in order to extend area coverage, detection range, and enhance KinPhy's sensitivity in the low SNR regime.

10 CONCLUSION

This paper proposes a novel in-band communication and sensing channel that utilises a programmable vibrating metasurface in order to allow a sensed device to send orthogonal kinetic information over a 60GHz link. With the increasing interest in mm-wave technology, our research furthers this body of work by opening the door to many new applications such as secure authentication and robust, long-range sensing for modern devices shipped with haptic capabilities. We give an overview of our prototype and characterise the performance in an indoor environment. Results show that our system can reliably sense minute vibrational information *irrespective* of the axial angles of the metasurface w.r.t. a reader radar, for distances up to 5m at >88% accuracy, and up to 3m at >90% accuracy.

ACKNOWLEDGMENTS

We thank our shepherd and anonymous reviewers for their valuable comments and time to improve the overall quality of this paper. We are grateful for Prof. Matt Reynolds of Washington University for his helpful feedback on the manuscript.

REFERENCES

[1] Fadel Adib, Hongzi Mao, Zachary Kabelac, Dina Katabi, and Robert C. Miller. 2015. Smart Homes That Monitor Breathing and Heart Rate. In *Proc. of the 33rd Annual ACM Conf. on Human Factors in Computing Systems (CHI '15)*. ACM, New York, NY, USA, 837–846.

[2] Mustafa Riza Akdeniz, Yuanpeng Liu, Mathew K Samimi, Shu Sun, Sundeep Rangan, Theodore S Rappaport, and Elza Erkip. 2014. Millimeter wave channel modeling and cellular capacity evaluation. *IEEE journal on selected areas in communications* 32, 6 (2014), 1164–1179.

[3] Sasan Bakhtiari, Thomas W Elmer, Nicholas M Cox, Nachappa Gopalsami, Appostolos C Raptis, Shaolin Liao, Ilya Mikhelson, and Alan V Sahakian. 2012. Compact millimeter-wave sensor for remote monitoring of vital signs. *IEEE Transactions on Instrumentation and Measurement* 61, 3 (2012), 830–841.

[4] Constantine A Balanis. 2016. *Antenna theory: analysis and design*. John wiley & sons.

[5] Omer Bayraktar, Ozlem Aydin Civi, and Tayfun Akin. 2012. Beam switching reflectarray monolithically integrated with RF MEMS switches. *IEEE Transactions on Antennas and Propagation* 60, 2 (2012), 854–862.

[6] Gregory L. Charvat. 2014. *Small and Short-Range Radar Systems* (1 ed.). CRC Press, Inc., Boca Raton, FL, USA.

[7] Victor C Chen, Fayin Li, S-S Ho, and Harry Wechsler. 2006. Micro-Doppler effect in radar: phenomenon, model, and simulation study. *IEEE Transactions on Aerospace and electronic systems* 42, 1 (2006), 2–21.

[8] F Falcone, T Lopetegi, MAG Laso, JD Baena, J Bonache, M Beruete, R Marqués, Ferran Martín, and M Sorolla. 2004. Babinet principle applied to the design of metasurfaces and metamaterials. *Physical review letters* 93, 19 (2004), 197401.

[9] Federal Communications Commission. [n. d.]. Spectrum Frontiers. https://docs.fcc.gov/public/attachments/FCC-16-89A1.pdf. Accessed: 10-03-19.

[10] Brian Ginsburg. 2018. F3: Circuits and architectures for wireless sensing, radar and imaging. In *IEEE International Solid-State Circuits Conference-(ISSCC)*. IEEE, 508–510.

[11] Karl Granstrom, Christian Lundquist, and Omut Orguner. 2012. Extended target tracking using a Gaussian-mixture PHD filter. *IEEE Trans. Aerospace Electron. Systems* 48, 4 (2012), 3268–3286.

[12] Muhammad Kumail Haider, Yasaman Ghasempour, Dimitrios Koutsonikolas, and Edward W Knightly. 2018. Listeer: mmwave beam acquisition and steering by tracking indicator leds on wireless aps. In *Proceedings of the 24th Annual International Conference on Mobile Computing and Networking*. ACM, 273–288.

[13] Mike Hazas and Andy Hopper. 2006. Broadband ultrasonic location systems for improved indoor positioning. *IEEE Transactions on mobile Computing* 5, 5 (2006), 536–547.

[14] IEEE Standards Association. 2012. IEEE Standard for Local and Metropolitan Area Networks-Part 15.6: Wireless Body Area Networks. *IEEE Standard for Information Technology* 802, 6 (2012), 1–271.

[15] Elliott Kaplan and Christopher Hegarty. 2005. *Understanding GPS: principles and applications*. Artech house.

[16] Heiji Kawai. 1969. The Piezoelectricity of Poly (vinylidene Fluoride). *Japanese Journal of Applied Physics* 8, 7 (jul 1969), 975–976. https://doi.org/10.1143/jjap.8.975

[17] Alexander V Kildishev, Alexandra Boltasseva, and Vladimir M Shalaev. 2013. Planar photonics with metasurfaces. *Science* 339, 6125 (2013), 1232009.

[18] Roberto Lerusalimschy, Waldemar Celes, and Luiz Henrique de Figueiredo. [n. d.]. Lua. https://www.lua.org. Accessed: 19-03-16.

[19] Jaime Lien, Nicholas Gillian, M. Emre Karagozler, Patrick Amihood, Carsten Schwesig, Erik Olson, Hakim Raja, and Ivan Poupyrev. 2016. Soli: Ubiquitous Gesture Sensing with Millimeter Wave Radar. *ACM Trans. Graph.* 35, 4, Article 142 (jul 2016), 142:1–142:19 pages.

[20] Adrian Loch, Hany Assasa, Joan Palacios, Joerg Widmer, Hans Suys, and Björn Debaillie. 2017. Zero Overhead Device Tracking in 60 GHz Wireless Networks using Multi-Lobe Beam Patterns. In *Proceedings of the 13th International Conference on emerging Networking EXperiments and Technologies*. ACM, 224–237.

[21] Wenjie Luo, Bin Yang, and Raquel Urtasun. 2018. Fast and Furious: Real Time End-to-End 3D Detection, Tracking and Motion Forecasting With a Single Convolutional Net. In *Proceedings of the IEEE Conference on Computer Vision and Pattern Recognition*. 3569–3577.

[22] Rene Mayrhofer. 2008. Ubiquitous Computing Security: Authenticating Spontaneous Interactions. Habilitation thesis, University of Vienna.

[23] Rene Mayrhofer and Hans Gellersen. 2007. On the Security of Ultrasound as Out-of-band Channel. In *Proc. IPDPS 2007: 21st IEEE International Parallel and Distributed Processing Symposium*. IEEE CS Press, Washington, DC, USA, 321. Track SSN 2007: 3rd International Workshop on Security in Systems and Networks.

[24] René Mayrhofer, Hans Gellersen, and Mike Hazas. 2007. Security by spatial reference: Using relative positioning to authenticate devices for spontaneous interaction. In *International Conference on Ubiquitous Computing*. Springer, 199–216.

[25] Ismail Nasr, Reinhard Jungmaier, Ashutosh Baheti, Dennis Noppeney, Jagjit S Bal, Maciej Wojnowski, Mustafa Emre Karagozler, Hakim Raja, Jaime Lien, Ivan Poupyrev, et al. 2016. A Highly Integrated 60 GHz 6-Channel Transceiver With Antenna in Package for Smart Sensing and Short-Range Communications. *J. Solid-State Circuits* 51, 9 (2016), 2066–2076.

[26] Novelda. 2018. XeThru X4M200 respiration sensor. https://www.xethru.com/x4m200-respiration-sensor.html Accessed: 19-03-16.

[27] Joan Palacios, Paolo Casari, and Joerg Widmer. [n. d.]. JADE: Zero-knowledge device localization and environment mapping for millimeter wave systems. In *IEEE INFOCOM 2017*. 1–9.

[28] Physik Instrumente GmbH & Co. [n. d.]. E-835 DuraAct Piezo Driver Module. https://www.pi-usa.us/fileadmin/user_upload/pi_us/files/product_datasheets/E835_Piezo_Controller_Electronics.pdf. Accessed: 19-03-16.

[29] Qualcomm. 2015. HP Pro Slate tablets rewrite the mobile experience with Snapdragon digital pen technology. https://www.qualcomm.com/news/onq/2015/01/20/hp-pro-slate-tablets-rewrite-mobile-experience-snapdragon-digital-pen-technology.

[30] Lenin Ravindranath, Calvin Newport, Hari Balakrishnan, and Samuel Madden. 2011. Improving wireless network performance using sensor hints. In *Proceedings of the 8th USENIX conference on Networked systems design and implementation*. 21–21.

[31] Reuters. [n. d.]. Google wins U.S. approval for new radar-based motion sensor. https://www.reuters.com/article/us-google-sensor/google-wins-u-s-approval-for-radar-based-hand-motion-sensor-idUSKCN1OV1SH. Accessed: 19-03-16.

[32] Hermann Rohling. 1983. Radar CFAR thresholding in clutter and multiple target situations. *IEEE transactions on aerospace and electronic systems* 4 (1983), 608–621.

[33] Swetank Kumar Saha, Hany Assasa, Adrian Loch, Naveen Muralidhar Prakash, Roshan Shyamsunder, Shivang Aggarwal, Daniel Steinmetzer, Dimitrios Koutsonikolas, Joerg Widmer, and Matthias Hollick. 2018. Fast and infuriating: Performance and pitfalls of 60 GHz WLANs based on consumer-grade hardware. In *2018 15th Annual IEEE International Conference on Sensing, Communication, and Networking (SECON)*. IEEE, 1–9.

[34] Stefan Schuster, Stefan Scheiblhofer, and Andreas Stelzer. 2009. The influence of windowing on bias and variance of DFT-based frequency and phase estimation. *IEEE Transactions on Instrumentation and Measurement* 58, 6 (2009), 1975–1990.

[35] Dan Sievenpiper, Lijun Zhang, Romulo FJ Broas, Nicholas G Alexopolous, and Eli Yablonovitch. 1999. High-impedance electromagnetic surfaces with a forbidden frequency band. *IEEE Transactions on Microwave Theory and techniques* 47, 11 (1999), 2059–2074.

[36] M.I. Skolnik. 1962. *Introduction to Radar Systems*. McGraw-Hill, New York, NY.

[37] Merrill Skolnik. 2002. *Systems aspects of digital beam forming ubiquitous radar*. Technical Report. Naval Research Lab, Washington DC.

[38] Milica Stojanovic and Lee Freitag. 2006. Multichannel detection for wideband underwater acoustic CDMA communications. *IEEE Journal of Oceanic Engineering* 31, 3 (2006), 685–695.

[39] Li Sui, Xin Xiong, and Gengchen Shi. 2012. Piezoelectric actuator design and application on active vibration control. *Physics Procedia* 25 (2012), 1388–1396.

[40] TDK Corp. 2018. PiezoHapt Actuators. https://product.tdk.com/info/en/products/sw_piezo/haptic/piezohapt/catalog.html.

[41] Texas Instruments Inc. [n. d.]. mmWave Studio. http://www.ti.com/tool/MMWAVE-STUDIO. Accessed: 19-03-16.

[42] Texas Instruments Inc. [n. d.]. Single-chip 60-GHz to 64-GHz intelligent mmWave sensor integrating processing capability. http://www.ti.com/product/IWR6843/toolssoftware. Accessed: 19-03-16.

[43] Texas Instruments Inc. 2018. mmWave Vital Signs Lab. https://training.ti.com/mmwave-vital-signs-lab.

[44] Francesco Tonolini and Fadel Adib. 2018. Networking across boundaries: enabling wireless communication through the water-air interface. In *Proceedings of the 2018 Conference of the ACM Special Interest Group on Data Communication*. ACM, 117–131.

[45] David Tse and Pramod Viswanath. 2005. *Fundamentals of Wireless Communications*. Cambridge University Press, Cambridge, UK.

[46] Vayyar Imaging Ltd. [n. d.]. Vayyar. https://vayyar.com. Accessed: 19-03-16.

[47] S Wang, AP Feresidis, G Goussetis, and JC Vardaxoglou. 2004. Low-profile resonant cavity antenna with artificial magnetic conductor ground plane. *Electronics Letters* 40, 7 (2004), 405–406.

[48] Shaogang Wang, Vishal M Patel, and Athina Petropulu. 2017. The Robust Sparse Fourier Transform (RSFT) and Its Application in Radar Signal Processing. *IEEE Trans. Aerospace Electron. Systems* 53, 6 (2017), 2735–2755.

[49] Saiwen Wang, Jie Song, Jaime Lien, Ivan Poupyrev, and Otmar Hilliges. 2016. Interacting with Soli: Exploring Fine-Grained Dynamic Gesture Recognition in the Radio-Frequency Spectrum. In *Proc. of the 29th Annual Symposium on User Interface Software and Technology (UIST '16)*. ACM, New York, NY, USA, 851–860. https://doi.org/10.1145/2984511.2984565

[50] Teng Wei, Anfu Zhou, and Xinyu Zhang. 2017. Facilitating robust 60 ghz network deployment by sensing ambient reflectors. In *14th {USENIX} Symposium on Networked Systems Design and Implementation ({NSDI} 17)*. 213–226.

[51] Zhicheng Yang, Parth H Pathak, Yunze Zeng, and Prasant Mohapatra. 2015. Sensor-assisted codebook-based beamforming for mobility management in 60 ghz wlans. In *2015 IEEE 12th International Conference on Mobile Ad Hoc and Sensor Systems*. IEEE, 333–341.

[52] Hui-Shyong Yeo, Gergely Flamich, Patrick Schrempf, David Harris-Birtill, and Aaron Quigley. 2016. Radarcat: Radar categorization for input & interaction. In *Proceedings of the 29th Annual Symposium on User Interface Software and Technology*. ACM, 833–841.

[53] Mingmin Zhao, Fadel Adib, and Dina Katabi. 2016. Emotion Recognition Using Wireless Signals. In *Proc. of the 22Nd Annual Int'l. Conf. on Mobile Computing and Networking (MobiCom '16)*. ACM, New York, NY, USA, 95–108.